CHEMISTRY
A EUROPEAN JOURNAL

DOI: 10.1002/chem.200500943

Density Control of Dodecamanganese Clusters Anchored on Silicon(100)

Guglielmo G. Condorelli,*[a] Alessandro Motta,[a] Maria Favazza,[a] Paola Nativo,[a] Ignazio L. Fragalà,[a] and Dante Gatteschi[b]

Abstract: A synthetic strategy to control the density of Mn_{12} clusters anchored on silicon(100) was investigated. Diluted monolayers suitable for Mn_{12} anchoring were prepared by Si-grafting mixtures of the methyl 10-undecylenoate precursor ligand with 1-decene spectator spacers. Different ratios of these mixtures were tested. The grafted surfaces were hydrolyzed to reveal the carboxylic groups available for the subsequent exchange with the $[Mn_{12}O_{12}(OAc)_{16}(H_2O)_4]\cdot 4H_2O\cdot 2AcOH$ cluster. Modified surfaces were analyzed by attenuated total reflection (ATR)-FTIR spectroscopy, X-ray photoemission spectroscopy (XPS), and AFM imaging. Results of XPS and ATR-FTIR spectroscopy show that the surface mole ratio between grafted ester and decene is higher than in the source solution. The surface density of the Mn_{12} cluster is, in turn, strictly proportional to the ester mole fraction. Well-resolved and isolated clusters were observed by AFM, using a diluted ester/decene 1:1 solution.

Keywords: cluster compounds · manganese · molecular magnets · monolayers · silicon

Introduction

Recent years have witnessed a progressive development in bottom-up technologies as alternative routes to top-down approaches for microelectronic applications. In fact, the continuous scaling down of the size of integrated circuits (IC) has had considerable limitations (lithographics, physics, or economics) for top-down technologies, whereas the bottom-up approach using molecules as single data-handling devices represents an enormous challenge in terms of storage and data-handling density. There are, thus, reports on molecular wires, switches, rectifiers, and storage elements that, in principle, might represent the basis of future molecular electronics.[1] The most promising architecture for molecular electronics is found in hybrid systems, in which a dense array of molecular devices is hosted on a silicon surface.[2] Monolayer formation, by self-assembling processes, on silicon surfaces certainly represents the most suitable route to developing hybrid systems.[3]

Some molecules can be used to store magnetic information. The most studied, prototypical molecule of this kind, referred to as a single molecular magnet (SMM), is a dodecamanganese(III/IV) cluster, $[Mn_{12}O_{12}(OAc)_{16}(H_2O)_4]\cdot 4H_2O\cdot 2AcOH$ (**1**$\cdot 4H_2O\cdot 2AcOH$).[4] A recent paper has shown the possibility of anchoring a thiol-substituted Mn_{12} cluster on gold substrate.[5] Patterned Mn_{12} aggregates have also been deposited from solution onto native silicon oxide, even though no clear-cut indication of a suitable bonding between the Si surface and the Mn_{12} cluster was provided.[6] The possibility of anchoring the Mn_{12} cluster on a surface of technological importance, such as Si(100), has been unambiguously demonstrated[7] in our laboratory by using ligand exchange with the bridging 10-undecylenic carboxylic acid grafted onto the Si surface through a strong Si–C bond (Figure 1).

Moreover, an important goal for the development of the Mn_{12} clusters in silicon technology as building blocks for magnetic-information storage relies upon the control of both the density and orientation of clusters on the silicon surface. Recently, a reproducible method to drive the orientation of thiol-substituted Mn_{12} clusters anchored on a gold substrate[8] and a possible approach to anchor oriented Mn_{12} on silicon[9] have been proposed.

In this paper, the possible control of the density of Mn_{12} clusters on silicon(100) is investigated. The adopted strategy

[a] Dr. G. G. Condorelli, Dr. A. Motta, M. Favazza, P. Nativo, Prof. I. L. Fragalà
Dipartimento di Scienze Chimiche
Università di Catania and INSTM
UdR Catania, Viale A. Doria 6, 95125 Catania (Italy)
Fax: (+39) 095-580-138
E-mail: guidocon@unict.it

[b] Prof. D. Gatteschi
Dipartimento di Chimica, Università di Firenze and INSTM
UdR di Firenze, Via della Lastruccia 3
50019 Sesto Fiorentino (Fi) (Italy)

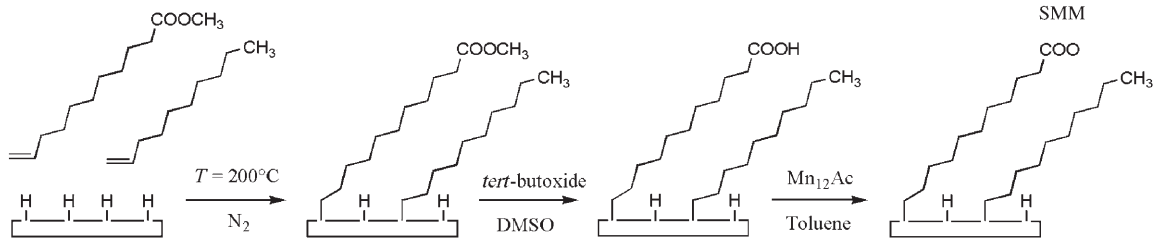

Figure 1. Three-step process for SMM anchoring on Si(100).

tunes the density of bridging functional carboxylate ligands on surfaces by using 1-decene as a spectator spacer. There is, in fact, evidence that negligible cluster sticking occurs on Si-grafted 1-decene monolayers.[7] Therefore, appropriate dilution of the exchangeable coordinating carboxylate bridge with spectator spacers represents a viable route to control the cluster density on the silicon surfaces. Modified surfaces were analyzed by X-ray photoemission spectroscopy (XPS), AFM imaging, and IR spectroscopy.

Results and Discussion

Diluted monolayers suitable for Mn_{12} anchoring were prepared by Si-grafting mixtures of different mole fractions of methyl 10-undecylenoate diluted with 1-decene: $\chi_{ester}(soln) =$ 0.0, 0.2, 0.5, 0.8, 1.0. The grafted surfaces were hydrolyzed and further treated by following an improved (relative to our earlier studies[7]) ligand-exchange strategy to anchor Mn_{12} clusters (Figure 1). Structures and compositional data of grafted monolayers before and after the Mn_{12} anchoring were analyzed by XPS and attenuated total reflection (ATR)-FTIR spectroscopy. AFM imaging provided further morphological information regarding the treated silicon surfaces.

X-ray photoemission spectroscopy: The XPS binding energy (*BE*) scale was calibrated by centering the Si $2p^{3/2}$ peak at 99.0 eV[10]. Figure 2 shows the Si signal of a fresh, HF-etched surface (a), of a pure decene monolayer (b), and of a pure ester monolayer before (c) and after (d) the Mn-anchoring step.

Following the monolayer grafting, the Si signal remains similar to that of the fresh, HF-etched Si surface for all χ_{ester}-(soln) values. There is evidence of the well-resolved Si $2p^{3/2-1/2}$ spin-orbit doublet of elemental silicon. The absence of any signal (at around 103 eV *BE*)[10] due to oxidized Si, even after some days of air exposure, points unequivocally (for all ester/decene ratios) to an efficient passivation of surfaces by the organic overlayer.

The relative intensity of the C 1s feature in the grafted samples is strongly enhanced in all cases, compared to the freshly HF-etched surface (Figure 2a–c). This accounts for the increased amount of carbon due to the organic layer. C 1s spectra of the pure ester, as well as of the diluted ester/decene samples, show rich structures, clearly due to several bonding states (Figure 2) at 287.3 (the methyl ester group $-O-CH_3$), 289.5 (the $>C=O$ carboxylic groups), 283.8 (the carbide Si–C bond), and 285.0 eV (the aliphatic backbone).[11] For the pure decene (Figure 2b), there are only two main components, centered at 283.8 and 285.0 eV.[11] A further component is always present at 286.0 eV, due to slightly oxidized carbon surface contaminants. This feature is ubiquitous in the present spectra and represents an artifact of chemical manipulations.

Similar to the C 1s features, the intensity of the O 1s envelope is markedly higher compared to the Si(100) freshly HF-etched surface (Figure 2) in the grafted layers for all samples. In all cases, the O 1s spectra show a component centered at 532.0 eV attributable to the oxidized silicon.[10] For the pure ester, as well as for the diluted surfaces, the O 1s band consists of two more components centered at 533.1 and 534.2 eV, which are assigned to the $>C=O$ and $=C-O-$ R groups, respectively, even though slightly higher *BE* values than those typically reported for polymers are observed (Figure 2c and d).[7,12] These bands are, of course, not present in the case of pure 1-decene (Figure 2b).

Table 1 and Figure 3 show the dependence of the intensities of the various C 1s and O 1s components upon the ester mole fraction $\chi_{ester}(soln)$. The relative (%) contributions f_x^C or f_x^O to the total intensities of either C 1s or O 1s features can be represented by the following equations;

$$f_x^C = I_x^C / I^C \times 100$$

$$f_x^O = I_x^O / I^O \times 100$$

in which I^C and I^O are the total spectral intensities and I_x^C and I_x^O denote intensities of the particular x component. The intensity ratios between the 289.5 and 287.3 eV carbon components are always 1:1, as expected for the grafted ester (Table 1). A similar trend is observed for the intensity ratio between the 534.2 and 533.1 eV oxygen components.

The relative intensities $f_{289.5}^C$ and $f_{534.2}^O$ vs $\chi_{ester}(soln)$ are reported in Figure 3. There is evidence that increased ester concentrations parallel the growth of relative intensities of the related O 1s and C 1s components centered at 289.5 and 534.2 eV, respectively.

In this context, the same $f_{289.5}^C$ and $f_{534.2}^O$ values become indicators of the surface ester concentrations $\chi_{ester}(surf)$, once normalized to homologous values of the pure ester (χ_{ester}-(soln) = 1.0). Figure 3b shows that surface concentrations of

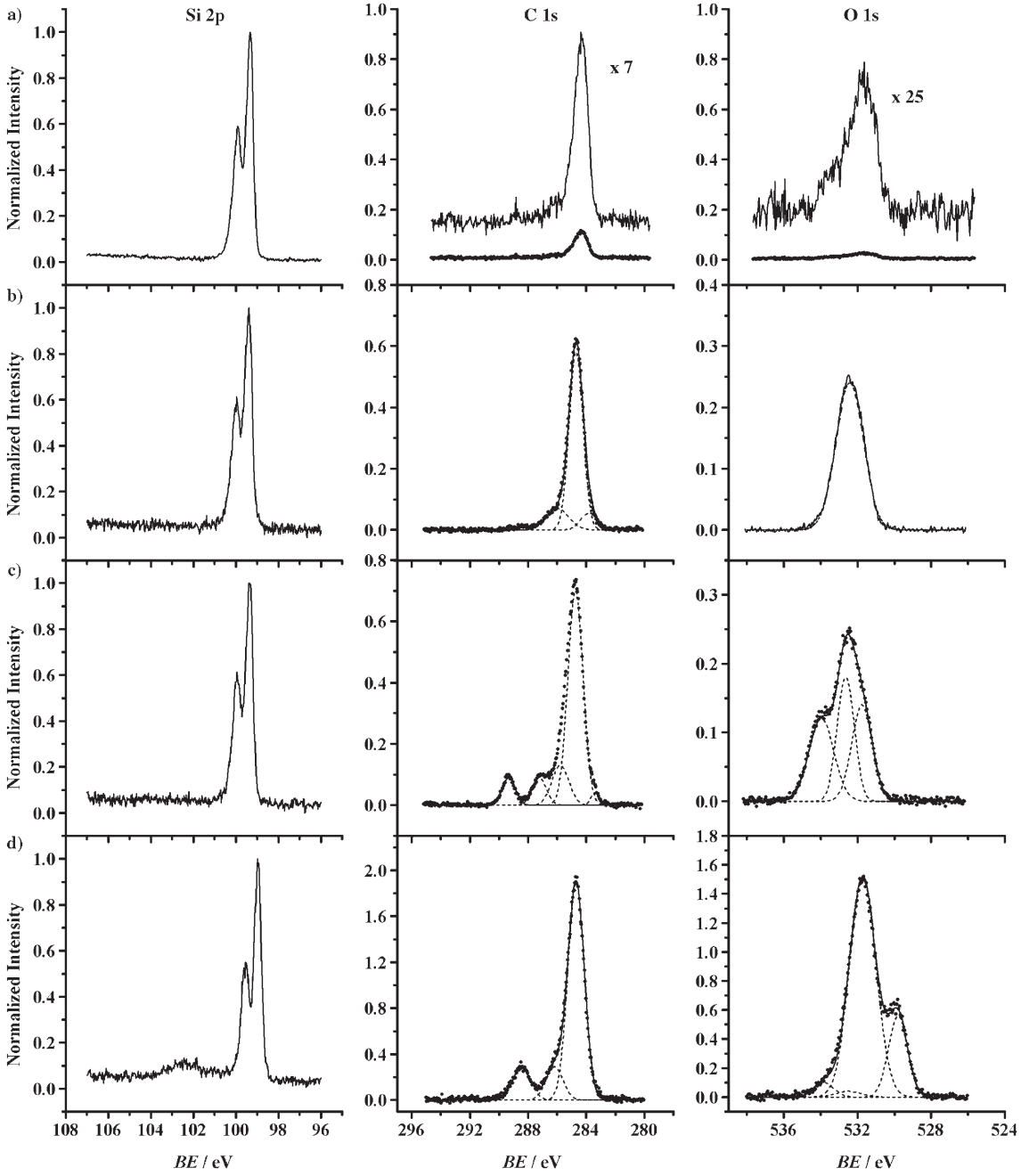

Figure 2. High-resolution XPS spectra of a) HF-etched Si(100) substrate, b) Si(100) substrates after grafting of the pure 1-decene, c) Si(100) substrates after grafting of the pure methyl 10-undecylenoate, d) Si(100) substrates after Mn_{12} anchoring. Left: Si 2p1s; center: C 1s; right: O 1s. The intensities are normalized to the total Si 2p intensity.

the grafting ester are greater than those in the precursor binary solutions.

Anchoring of the Mn clusters (after the ester hydrolysis) causes remarkable changes to the XPS spectral regions relative to simpler grafted ester/decene layers (Figure 2d). Thus, the Si 2p region shows two distinct features: a well-defined $2p^{3/2-1/2}$ doublet (at 99.0 and 99.6 eV, respectively) associated with the elemental silicon (Si^0), and a weak, broad band at 102.5 eV, representing oxidized silicon species (SiO_x), due to either hydrolysis or the ligand-exchange step. The C 1s features (Figure 2d) have increased relative intensities and show a clear shift of the carboxylic component (289.5 eV)[11] toward lower binding energies (288.8 eV), as expected for the carboxylate $-COO^-$ groups[13] present in both the bridging acetate ligands in Mn_{12} and in the 10-undecyl grafted carboxylate. Note, however, that the broadening of this band may hide any low-intensity component at 289.5 eV that is still present because of a possible partial ligand exchange. Finally, the shoulder at 283.8 eV is no longer visible, due to the increased thickness of the grafted layer. These

Table 1. Distribution of carbon and oxygen (%) over their components vs ester/decene ratios.

χ_{ester}(soln)	C 1s components					O 1s components		
	$f^{C}_{289.5}$	$f^{C}_{287.3}$	$f^{C}_{285.0}$	$f^{C}_{283.8}$	$f^{C}_{286.0}$	$f^{O}_{534.2}$	$f^{O}_{533.1}$	$f^{O}_{532.0}$
0.0	0.0	0.0	77.6	6.0	16.4	0.0	0.0	100.0
0.2	3.5	3.5	72.9	3.6	16.4	11.5	11.5	77.0
0.5	4.9	4.9	67.7	4.1	18.4	24.4	24.4	51.2
0.8	6.9	6.9	64.3	3.1	18.8	29.3	29.3	41.4
1.0	7.8	7.8	66.9	2.1	15.3	34.0	34.0	32.0

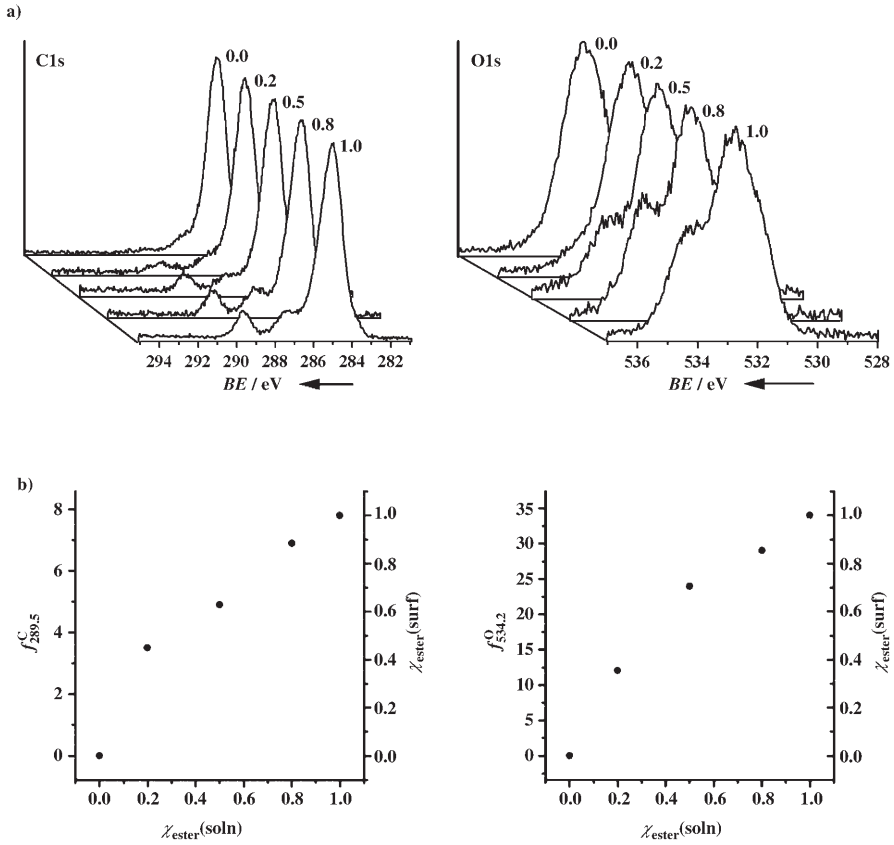

Figure 3. a) C 1s and O 1s band regions for the grafted surfaces at different ester/decene mole fractions. b) Plots of $f^{C}_{289.5}$ and $f^{O}_{534.2}$ vs mole fraction of methyl 10-undecylenoate in the binary precursor deposition solutions. The right axes represent the corresponding surface mole fractions χ_{ester}(surf).

considerations, of course, do not apply to pure decene overlayers, because Mn_{12} anchoring is precluded.[7]

In the SMM layer, the O 1s features have increased intensities and, both for pure ester and for ester/decene diluted surfaces, are resolved into four components (Figure 2d). The bands centered at 530.4 and 532.3 eV have been assigned to the $Mn_{12}O_{12}$ core and to the remaining 36 oxygen atoms of the ligand framework.[4] The ~1:3 intensity ratio between the 530.4 and 532.3 eV O 1s components agrees well with the expected substitution efficiency (Table 2). The third component (at 532.8 eV) remains associated with oxidized silicon. The fourth component (at 534.1 eV) represents unreacted ester groups in accordance with the broadening of the carbon component centered at 289.5 eV. In the case of the pure decene surface, no sizeable change in the O 1s signal can be observed after the Mn-anchoring step.

The Mn valence state in the SMM layer was investigated by exploiting the peculiarities of the XPS features of Mn 3s. The Mn 3s band splitting, due to exchange coupling between the 3s hole and the 3d electrons, is the best indicator of the Mn valence state.[14] Thus, the observed value (5.1 eV) is consistent with a formal valence ranging from 3+ to 3.3+, as expected for Mn_{12}.

Table 2 and Figure 4 show that, upon increasing the ester mole fraction, parallel increases in relative intensities of the oxygen components centered at 530.4 and 532.3 eV associated with the Mn_{12} cluster are observed. A similar trend is also visible for the carbon component centered at 288.8 eV, associated with the carboxylate $-COO^{-}$ groups present in both acetate and 10-undecyl bridging carboxylate ligands (see above). Similarly, the I^{Mn} intensity of the Mn $2p^{3/2}$ feature relative to that of Si 2p increases in parallel with the increase in the ester mole fraction in the grafting solution and, hence, in parallel with the surface concentration of carboxylic groups (Figure 5). This trend accords well with a greater Mn_{12} surface concentration.

Table 2. I^{Mn}/I^{Si} intensity ratio and distribution of carbon and oxygen (%) over their components vs ester/decene ratios, after the Mn-anchoring step.

χ_{ester}(soln)	I^{Mn}/I^{Si}	$f^{C}_{288.8}$	$f^{C}_{285.0}$	$f^{C}_{286.5}$	$f^{O}_{534.1}$	$f^{O}_{532.8}$	$f^{O}_{532.3}$	$f^{O}_{530.4}$
0.0	0.00	0.0	80.7	19.3	0.0	100.0	0.0	0.0
0.2	0.14	6.8	81.4	11.8	4.6	60.9	25.9	8.6
0.5	0.27	8.6	77.1	9.5	2.0	40.1	43.4	14.5
0.8	0.49	10.3	75.6	14.1	2.2	23.5	55.7	18.6
1.0	0.54	12.2	75.7	12.1	2.6	11.4	64.5	21.5

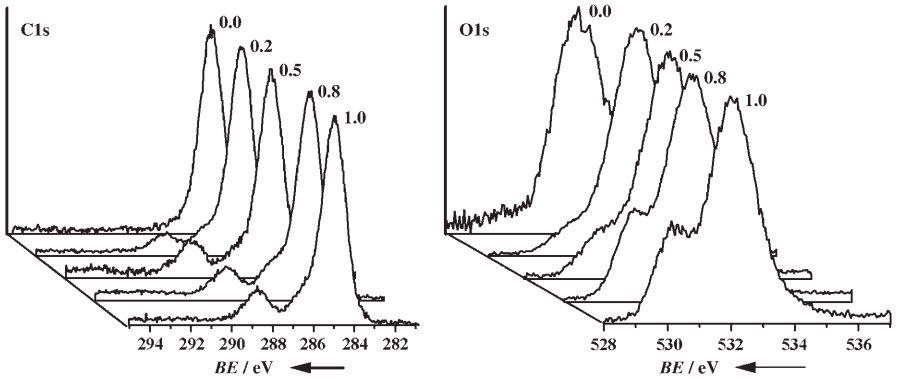

Figure 4. C 1s and O 1s band regions of grafted surfaces at different ester/decene mole fractions after the Mn_{12}-anchoring step.

as no angle dependence is observed. However, as expected for a Mn-containing overlayer homogeneously distributed on the substrate, the I^{Mn}/I^{Si} ratio progressively increases as the takeoff angle is decreased.[7]

Infrared absorption spectroscopy: ATR-FTIR spectroscopy was used to monitor the entire Mn-anchoring process. Figure 7 shows the ATR-FTIR spectrum in the region of interest for Si–H surface vibrations (2000–

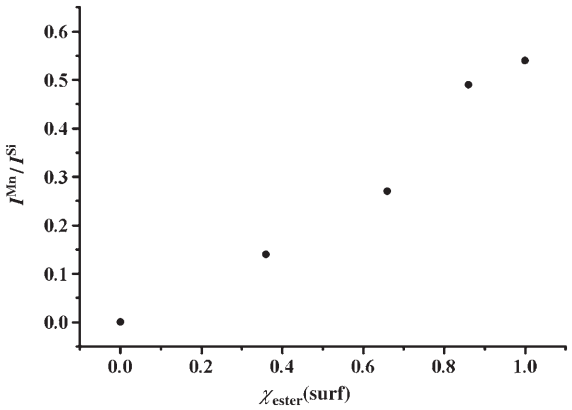

Figure 5. The I^{Mn}/I^{Si} intensity ratio vs the surface mole fraction of methyl 10-undecylenoate, χ_{ester}(surf).

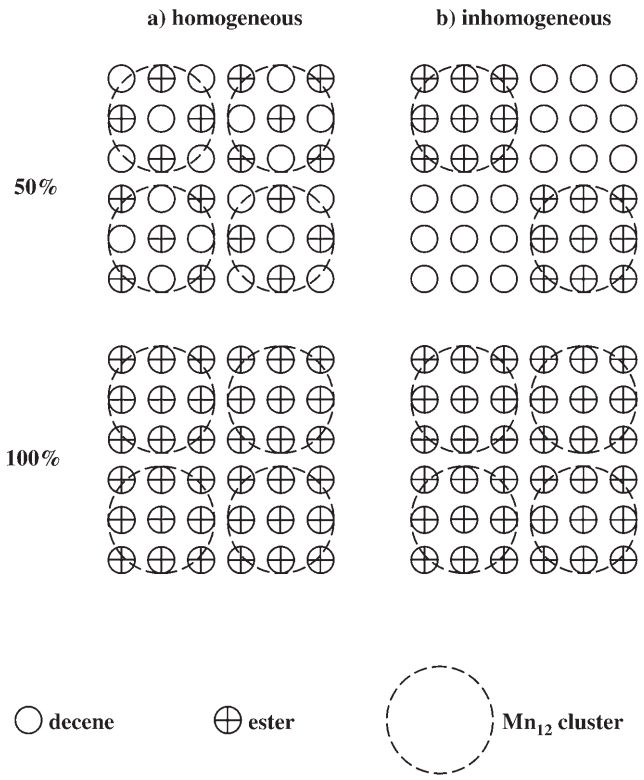

Figure 6. Prototypical diagrams of Mn_{12} coverage on a) homogeneously mixed ester/decene monolayers, b) inhomogeneously mixed ester/decene monolayers.

This observation is not, however, consistent with a homogeneously mixed ester/decene monolayer. The maximum value of the surface ester concentration is greater than that of the Mn_{12} surface concentration, due to the difference in molecular sizes. In particular, the cross-sectional area commonly measured for alkyl chains in packed monolayer (20 Å^2)[15] is much lower than the estimated cross-sectional area of the Mn_{12} cluster (~150 Å^2).[16] Therefore, for a homogeneously mixed ester/decene monolayer, naive structural considerations (Figure 6a) clearly indicate that Mn_{12} full coverage can be obtained for both $\chi_{ester}(surf) = 0.5$ and $\chi_{ester}(surf) = 1$. By contrast, in the case of a prototypical inhomogeneous ester/decene coverage (Figure 6b), the surface Mn_{12} concentration depends on the χ_{ester}(surf).

Angle-resolved XPS measurements of diluted monolayers are fully consistent with our earlier results.[7] Thus, C 1s and O 1s regions show a progressive increase in intensities of the components, due to the carboxylic group and the decrease of the Si–C component upon reduction in the takeoff angle. These results are consistent with a grafting Si–C bond and with an ester group atop the layer. After the Mn anchoring, analysis of the C 1s regions indicates an isotropic distribution of the carboxylic ligands (10-undecylenate and acetate),

2200 cm^{-1}) following the etching treatment. Three bands centered at 2135, 2105, and 2085 cm^{-1} (associated with the SiH_3, SiH_2, and SiH stretching, respectively)[17] are visible. This is indication of a highly efficient etching treatment to produce Si–H terminated surface.

After the grafting reaction, two spectral regions become diagnostic, namely that of CH stretching between 3200 and 2700 cm^{-1} and that of carbonyl stretching at around 1740 cm^{-1} (for the pure ester and for the ester/decene diluted samples (Figure 8)). Of course, in the case of the pure

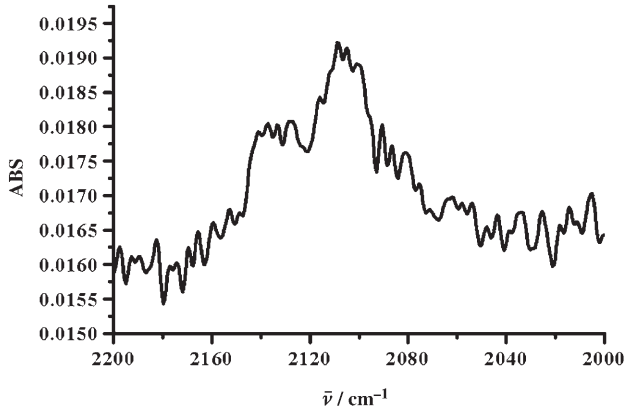

Figure 7. ATR-FTIR absorption spectrum of the Si(100) surface in the Si–H region after etching.

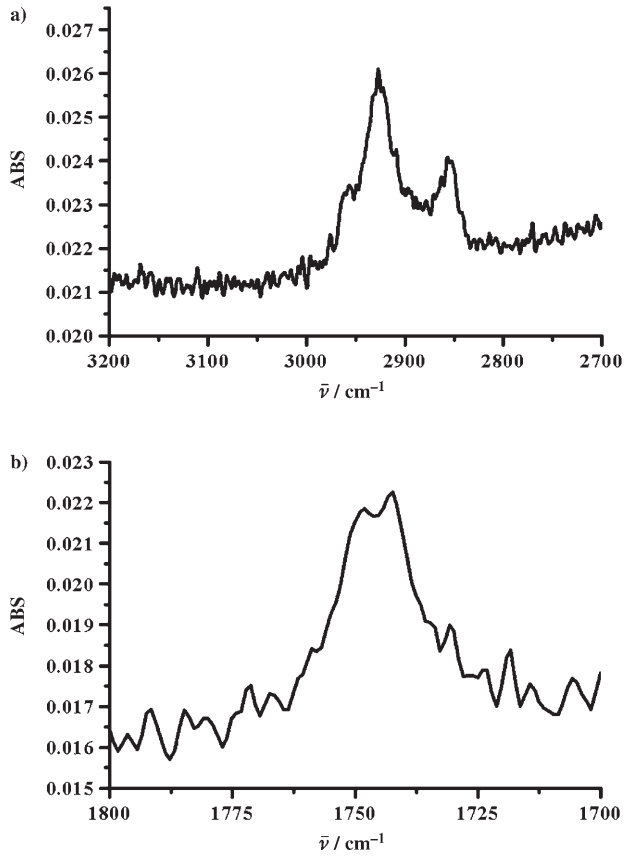

Figure 8. ATR-FTIR spectra of Si(100) surfaces after grafting with pure methyl 10-undecylenoate: a) C–H region, b) carbonyl region. In both cases, the background due to the substrate has been subtracted.

decene overlayer, only the CH stretching region shows the expected features.

This spectral region is, however, similar for all grafted monolayers. Thus, the feature at 2958–2960 cm^{-1} represents the CH_3 asymmetric in-plane CH stretching mode, due to vibrations of both esteric $-OCH_3$ and methyl groups of 1-decyl chains.[18] The bands at 2926–2927 and 2856–2857 cm^{-1} are assigned to the $\nu_a(CH_2)$ and $\nu_s(CH_2)$ stretching modes, respectively. In the case of pure ester, as well as the diluted overlayers, a band centered at 1740 cm^{-1}, unambiguously assigned to the C=O stretch of ester groups, becomes visible.

After the Mn-anchoring step, the band at 1740 cm^{-1} disappears and three bands centered at 1560, 1428, and 1710 cm^{-1} are visible (Figure 9). These bands are assigned to the

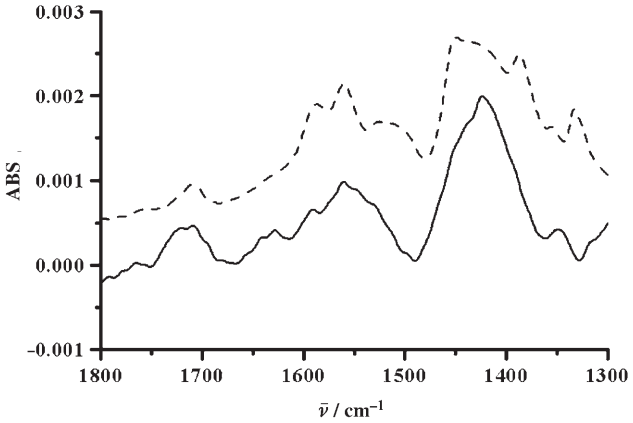

Figure 9. IR features of the grafted surface following the Mn-anchoring process after subtraction of the SiO_2 background. The dotted line displays the spectrum of the free Mn complex in KBr powders used as reference.

COO^- group symmetrical stretching mode (1560 and 1428 cm^{-1}) and to unreacted acid groups (1710 cm^{-1}).[19] Note that the spectrum is totally coincident with that of the $[Mn_{12}O_{12}(OAc)_{16}(H_2O)_4]\cdot 4H_2O\cdot 2$ AcOH powder.

Figure 10 shows the absorbance ratios between the bands at 1740 and 2936 cm^{-1} of monolayers on silicon(100), depending on the ester mole fraction in the grafting (ester/decene) agent. As expected, the intensity of the band at 1740 cm^{-1} increases monotonically, in parallel to the increasing ester mole fraction of the grafting solution.

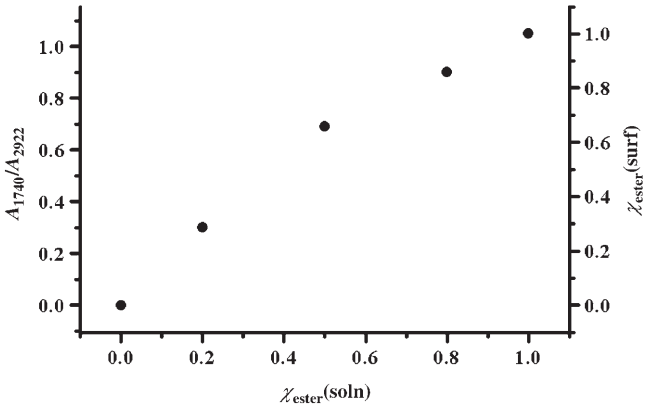

Figure 10. Absorbance ratios A_{1740}/A_{2922} of diluted ester/decene monolayers on silicon after grafting with mixtures of methyl 10-undecylenoate and 1-decene. The trend vs χ_{ester}(surf) is also reported.

As for the XPS data described above, the surface ratio between the two grafting agents, $\chi_{ester}(surf)$, can be safely evaluated by normalizing the A_{1740}/A_{2922} ratios to that of the pure methyl 10-undecylenoate, assumed as the reference unit ($\chi_{ester}(soln)=1.0$). This reinforces our early contention that the surface density of functional groups can be finely tuned by simply varying the composition of the grafting solution.

Atomic force microscopy: The roughness and morphological homogeneity of the present overlayers were evaluated by AFM. Figure 11 shows how the surface morphologies depend on $\chi_{ester}(surf)$ values. Prototypical cases ($\chi_{ester}(surf)=$ 0.0, 0.7, 1.0) are displayed to show the most remarkable morphological differences. Consideration of images (Figure 11) and of usual statistical parameters (the mean particle height R_{mean} and the surface roughness R.M.S.), indicates the most relevant surface modifications due to Mn_{12} cluster anchoring. The self-assembled (S.A.) layer before cluster anchoring (Figure 11a) appears, in all cases, very flat and homogeneous with a roughness (R.M.S. = 0.05 nm) and a R_{mean} value (0.16 nm) comparable to those of a freshly etched Si(100) surface.

After grafting the Mn_{12} clusters, more structured morphologies (than that of the host S.A. surface) are observed. There is evidence of poorly ordered particles, almost homogeneously distributed over the surface. In the case of diluted S.A. host ($\chi_{ester}(surf)=0.5$), the Mn_{12} clusters are well resolved and isolated (Figure 11b). The typical vertical size of the observed features (R_{mean}) in this case is about 1 nm, consistent with the expected height of cluster **1**.

The roughness (R.M.S. = 0.21) clearly increases relative to the unreacted ester surface, due to the cluster architecture. The apparent lateral size is about 10 nm, which is greater than the expected value (about 1 nm) for the isolated Mn_{12} cluster. Nevertheless, this is a probable artifact caused by the limited lateral resolution of the AFM analysis.

Surfaces with pure esteric S.A. layers ($\chi_{ester}(surf)=1.0$) show rather unresolved morphologies after Mn_{12} grafting, possibly due to formation of cluster aggregates (Figure 11c). This contention is supported by the vertical size of related AFM features ($R_{mean}=1.3$ nm) and by the roughness value (R.M.S. = 0.3). Cluster aggregation is similarly responsible for the increased lateral size (20–25 nm) measured in this case.

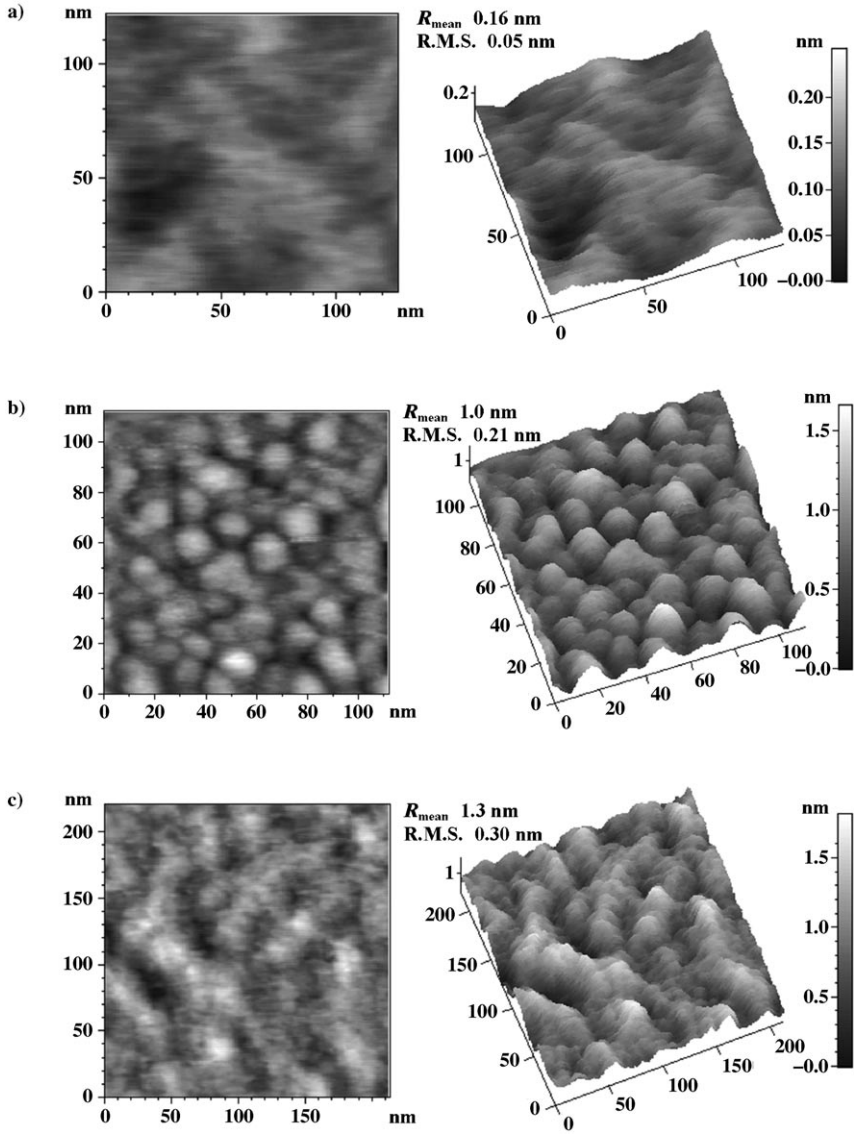

Figure 11. AFM images of a) S.A. layer before cluster anchoring, b) S.A. diluted layer ($\chi_{ester}(surf)=0.7$) after cluster anchoring, c) S.A. layer ($\chi_{ester}(surf)=1.0$) after cluster anchoring. The different lateral scale is adopted to display better the structured surface. In all cases, the 2D image is displayed on the left and the 3D image on the right.

Conclusion

The possibility of an accurate control of the surface density of Mn_{12} cluster on silicon(100) was investigated by tuning the surface concentration of grafting carboxylate groups. XPS and ATR-FTIR spectroscopy data confirm that the surface concentration $\chi_{ester}(surf)$ of the grafting methyl 10-undecylen-

oate depends on the mole ratio χ_{ester}(soln) of the precursor binary solution to the 10-decene spectator. The χ_{ester}(surf) values, independently evaluated by XPS and ATR measurements, indicate a sizeable (relative to the solution) enrichment of surface ester concentration. XPS results taken after the Mn_{12} anchoring show that the Mn/Si intensity ratio increases in parallel to the increasing ester mole fraction. AFM morphologies critically depend on the surface Mn_{12} concentration. Thus, almost flat surfaces are observed for unreacted Si(100) surfaces before Mn_{12} anchoring. Well-resolved structure, consistent with the Mn_{12} dimensionality (vertical size of the observed features (R_{mean}) of about 1 nm), are observed for diluted (χ_{ester}(surf) = 0.7) surfaces. Overcrowded surfaces (χ_{ester}(surf) = 1.0) cause poorly resolved nanostructuring, due to the formation of cluster aggregates.

Experimental Section

All chemicals, unless otherwise noted, were commercially available and were used as received. Solvents for substrate cleaning were distilled, 1-decene for monolayer preparation was distilled under reduced pressure over Na metal.

The XPS spectra were obtained by using a PHI ESCA/SAM 5600 Multitechnique spectrometer equipped with a monochromatized $Al_{K\alpha}$ X-ray source. The analyses were carried out at various photoelectron angles (relative to the sample surface) in the 10–80° range with an acceptance angle of ±7°.

AFM images were obtained in high-amplitude mode (tapping mode) by using a NT-MTD instrument apparatus. The noise level before and after each measurement was 0.01 nm.

Infrared spectra of the monolayers were recorded by using a Harrick GATR germanium single-reflection ATR accessory. The spectra were collected with 800 scans at 2 cm^{-1} resolution.

$[Mn_{12}O_{12}(OAc)_{16}(H_2O)_4]\cdot 4H_2O\cdot 2$ AcOH was synthesized according to the literature;[3] ^{1}H NMR (500 MHz, CD_3CN, 25 °C, TMS): $\delta = 47$ (12 H; axial Mn^{III}–Mn^{III}), 40 (24 H; equatorial Mn^{III}–Mn^{III}), 14 ppm (12 H; axial Mn^{III}–Mn^{IV}); elemental analysis calcd (%) for $C_{36}H_{72}O_{56}Mn_{12}$: C 20.97, H 3.52; found: C 21.01, H 3.24.

Methyl 10-undecylenoate was synthesized according to the method reported by Sieval et al.[20] Briefly, a mixture of 10-undecylenic acid (10 g, 54 mmol), methanol (65 mL), and sulfuric acid (0.14 mL) was refluxed for 3 h. The excess methanol was removed in vacuum, and the resulting material was dissolved in ether. The product was distilled under vacuum to obtain a transparent liquid. ^{1}H NMR (500 MHz, $CDCl_3$, 25 °C, TMS): $\delta = 5.83$–5.78 (m, 1 H), 5.00–4.91 (m, 2 H), 3.66 (s, 3 H), 3.31–2.84 (m, 2 H), 2.06–2.01 (m, 2 H), 1.63–1.9 (m, 2 H), 1.38–1.29 ppm (m, 10 H).

Monolayer preparation: The alkene solution, methyl 10-undecylenoate/1-decene (10 mL), was placed in a small, three-necked flask fitted with a nitrogen inlet and a condenser. The solution was deoxygenated with dry nitrogen for at least 1 h. Subsequently, a Si(100) substrate was treated in a piranha solution for 12 min, rinsed in water for 2 min, and etched in 1.0% hydrofluoric acid for 90 s, then immediately placed in the alkene solution. The solution was then refluxed at 200 °C for 2 h, under slow N_2 bubbling to prevent bumping. After cooling to RT, the sample was removed from the flask and sonicated in dichloromethane for 10 min.

Hydrolysis of methyl 10-undecylenoate was performed by treatment with potassium *tert*-butoxide in DMSO,[21] according to a method reported by Strother et al.[22] Briefly, the grafted surfaces were dipped into a solution of potassium *tert*-butoxide in DMSO (250 mM) for 30 s at RT, then rinsed in acidified water (100 mM HCl).

The Mn_{12}-functionalized silicon surface was prepared by a modified ligand-exchange method.[23] The silicon surface was rinsed in a slurry of freshly-prepared $[Mn_{12}O_{12}(OAc)_{16}(H_2O)_4]\cdot 4H_2O\cdot 2$ AcOH in anhydrous toluene blown dry with nitrogen. The reaction was performed in a glove box for 2 h at RT. The modified substrate was removed from the solution and sonicated in acetonitrile and dichloromethane for 10 min to remove unreacted Mn_{12} clusters.

Acknowledgements

The authors thank the Ministero Istruzione Università e Ricerca (MIUR, Roma) for financial support (PRIN and FIRB projects).

[1] G. P. Lopinski, D. D. M. Wayner, R. A. Wolkow, *Nature* **2000**, *406*, 48–51.
[2] G. F. Cerofolini, G. Ferla, *J. Nanopart. Res.* **2002**, *4*, 185–191.
[3] a) M. R. Linford, P. Fenter, P. M. Eisemberger, C. E. D. Chidsey, *J. Am. Chem. Soc.* **1995**, *117*, 3145–3155; b) J. M. Buriak, *Chem. Rev.* **2002**, *102*, 1271–1308; c) D. D. Wayner, R. A. Wolkow, *J. Chem. Soc. Perkin Trans. 1* **2002**, *2*, 23–34.
[4] a) T. Lis, *Acta Crystallogr. Sect. B* **1980**, *36*, 2042–2046; b) R. Sessoli, D. Gatteschi, A. Caneschi, M. A. Novak, *Nature* **1993**, *365*, 141–143; c) G. Christou, D. Gatteschi, D. N. Hendrickson, R. Sessoli, *Mater. Res. Bull.* **2000**, *35*, 66–71.
[5] A. Cornia, A. C. Fabretti, M. Pacchioni, L. Zobbi, D. Bonacchi, A. Caneschi, D. Gatteschi, R. Biagi, U. del Pennino, V. De Renzi, L. Gurevich, H. S. J. van der Zant, *Angew. Chem.* **2003**, *115*, 1683–1686; *Angew. Chem. Int. Ed.* **2003**, *42*, 1645–1648.
[6] M. Cavallini, F. Biscarini, J. Gomez-Segura, D. Ruiz, J. Veciana *Nano Lett.* **2003**, *3*, 1527–1530.
[7] G. G. Condorelli, A. Motta, I. L. Fragalà, F. Giannazzo, V. Raineri, A. Caneschi, D. Gatteschi, *Angew. Chem.* **2004**, *116*, 4173–4176; *Angew. Chem. Int. Ed.* **2004**, *43*, 4081–4084.
[8] M. Pacchioni, A. Cornia, A. C. Fabretti, L. Zobbi, D. Bonacchi, A. Caneschi, G. Chastanet, D. Gatteschi, R. Sessoli, *Chem. Commun.* **2004**, *22*, 2604–2605.
[9] B. Fleury, L. Catala, V. Huc, C. David, W. Z. Zhong, L. B. Jegou, P.-A. Palacin, T. Mallah, *Chem. Commun.* **2005**, 2020–2022.
[10] a) G. F. Cerofolini, C. Galati, S. Lorenti, L. Renna, O. Viscuso, C. Bongiorno, V. Raineri, C. Spinella, G. G. Condorelli, I. L. Fragalà, A. Terrasi, *Appl. Phys. A* **2003**, *77*, 403–409; b) G. F. Cerofolini, C. Galati, L. Renna, N. Re, *Appl. Phys. A* **2003**, *77*, 515–521.
[11] a) D. Briggs, G. Beamson, *Anal. Chem.* **1992**, *64*, 1729–1736; b) D. Briggs in *Practical Surface Analysis, Vol. 1: Auger and X-ray Photoelectron Spectroscopy*, 2nd ed. (Eds.: D. Briggs, M. P. Seah), John Wiley, Chichester, **1995**, pp. 444–454; c) G. F. Cerofolini, C. Galati, S. Reina, L. Renna, G. G. Condorelli, I. L. Fragalà, G. Giorni, A. Sgamellotti, N. Re, *Appl. Surf. Sci.* **2005**, *246*, 52–67.
[12] D. Briggs, G. Beamson, *Anal. Chem.* **1993**, *65*, 1517–1523.
[13] a) J. S. Hammond, J. W. Holubka, J. E. Devries, R. A. Duckie, *Corros. Sci.* **1981**, *21*, 239–253; b) A. M. Dennis, R. A. Howard, K. M. Kadish, J. L. Bean, J. Brace, N. Winograd, *Inorg. Chim. Acta* **1980**, *44*, L139–L141; c) V. I. Nefedov, Y. V. Salyn, X. Keller, *Zh. Neorg. Khim.* **1979**, *24*, 2564–2566.
[14] a) V. R. Galakhov, M. Demeter, S. Bartkowski, M. Neumann, N. A. Ovechkina, E. Z. Kurmaev, N. I. Lobachevskaya, Ya. M. Mukovskii, J. Mitchell, D. L. Ederer, *Phys. Rev. B* **2002**, *65*, 113102/1–113102/4; b) V. Di Castro, G. Polzonetti, *J. Electron Spectrosc. Relat. Phenom.* **1989**, *48*, 117–123.
[15] E. U. Thoden van Velzen, J. F. J. Engbersen, P. J. de Lange, J. W. G. Mahy, D. N. Reinhoudt, *J. Am. Chem. Soc.* **1995**, *117*, 6853–6862.
[16] A. Cornia, A. C. Fabretti, R. Sessoli, L. Sorace, D. Gatteschi, A. L. Barra, C. Daiguebonne, T. Roisnel, *Acta Crystallogr. Sect. C* **2002**, *C58*, m371 m373.

[17] a) M. Shinohara, M. Niwano, Y. Neo, K. Yokoo, *Thin Solid Films* **2000**, *369*, 16–20; b) Y. J. Chabal, G. S. Higashi, K. Raghavachari, V. A. Burrows, *J. Vac. Sci. Technol. A* **1989**, *7*, 2104–2109.
[18] D. Lin-Vien, N. B. Colthup, W. G. Fateley, J. G. Grasselli in *The Handbook of Infrared and Raman Characteristic Frequencies of Organic Molecules*, Academic Press, San Diego, CA, **1991**, pp. 134–141.
[19] K. Nakamoto in *Infrared and Raman Spectra of Inorganic and Coordination Compounds*, 3rd ed., John Wiley, New York, **1978**, pp. 231–232.
[20] A. B. Sieval, A. L. Demirel, J. M. Nissink, M. R. Linford, J. H. van der Maas, W. H. de Jeu, H. Zuilhof, E. J. R. Sudhölter, *Langmuir* **1998**, *14*, 1759–1768.
[21] a) F. C. Chang, N. F. Wood, *Tetrahedron Lett.* **1964**, *5*, 2969–2973; b) P. G. Gassman, W. N. Shenk, *J. Org. Chem.* **1977**, *42*, 918–920.
[22] T. Strother, W. Cai, X. Zhao, R. J. Hamers, L. M. Smith, *J. Am. Chem. Soc.* **2000**, *122*, 1205–1209.
[23] H. J. Eppley, H.-L. Tsai, N. de Vries, K. Folting, G. Christou, D. N. Hendrickson, *J. Am. Chem. Soc.* **1995**, *117*, 301–317.

Received: August 3, 2005
Revised: November 22, 2005
Published online: February 21, 2006

